Electronic Supplementary Material (ESI) for Environmental Science: Nano.

Clearance of nanoparticles from blood: Effects of hydrodynamic size and surface coatings

Bingqing Lu[1*], Jiaqi Wang [1], A. Jan. Hendriks[1], Tom M. Nolte[1]

[1]Department of Environmental Science, Institute for Biological and Environmental Sciences, Radboud University Nijmegen, 6500 GL Nijmegen, The Netherlands

* Corresponding author: bingqing.lu@ru.nl

Contents

Fig. S1. The curve fitting of all NPs data by one- (black curve) and two-compartment (blue curve) kinetics.

1. Methods

1.1 The derivation of total rate constants

1.2 Clearance rate constants based on *Van der Waals* energy

Table S1. The fitting results of data for parameterization and validation based on one- and two-compartment kinetics.

Table S2. Chemical information of NPs coatings (including 7 data points for parameterization and 4 data points for validation (in bold)).

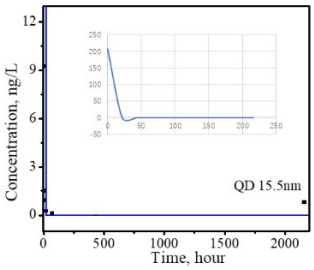
QD 15.5nm
Concentration, ng/L
Time, hour

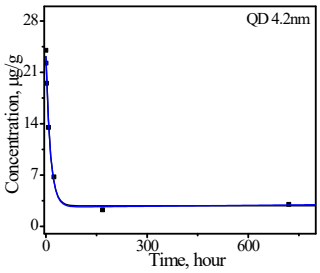
QD 4.2nm
Concentration, µg/g
Time, hour

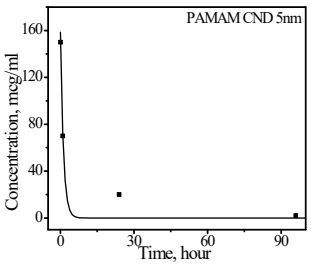
PAMAM CND 5nm
Concentration, mcg/ml
Time, hour

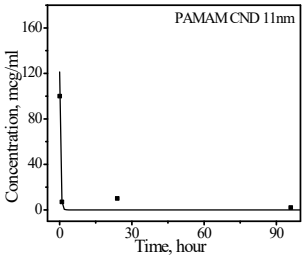
PAMAM CND 11nm
Concentration, mcg/ml
Time, hour

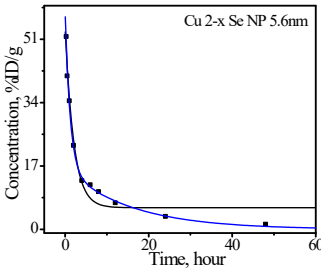
Cu 2-x Se NP 5.6nm
Concentration, %ID/g
Time, hour

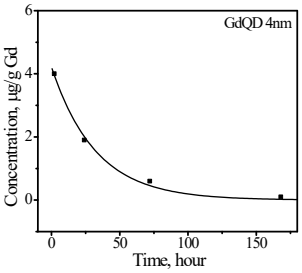
GdQD 4nm
Concentration, µg/g Gd
Time, hour

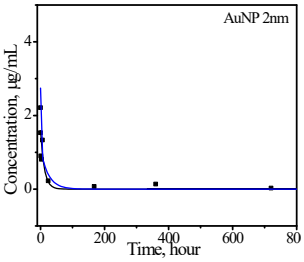
AuNP 2nm
Concentration, µg/mL
Time, hour

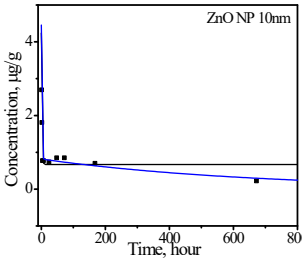
ZnO NP 10nm
Concentration, µg/g
Time, hour

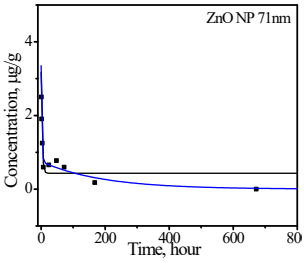
ZnO NP 71nm
Concentration, µg/g
Time, hour

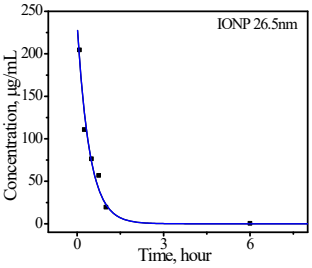
IONP 26.5nm
Concentration, µg/mL
Time, hour

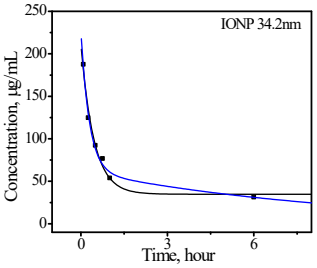
IONP 34.2nm
Concentration, µg/mL
Time, hour

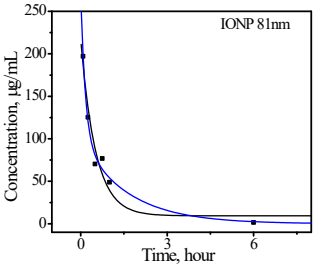
IONP 81nm
Concentration, µg/mL
Time, hour

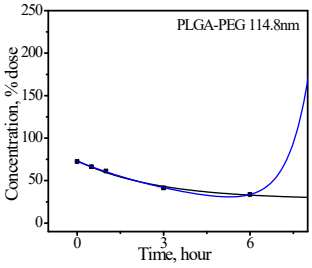
PLGA-PEG 114.8nm
Concentration, % dose
Time, hour

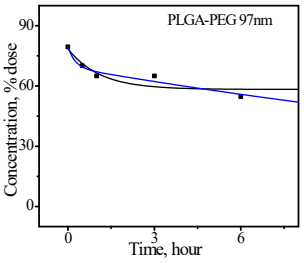
PLGA-PEG 97nm
Concentration, % dose
Time, hour

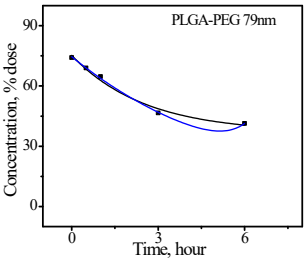
PLGA-PEG 79nm
Concentration, % dose
Time, hour

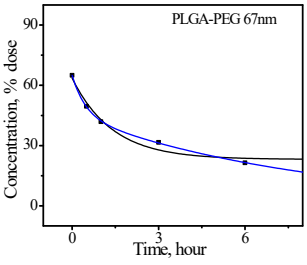
PLGA-PEG 67nm
Concentration, % dose
Time, hour

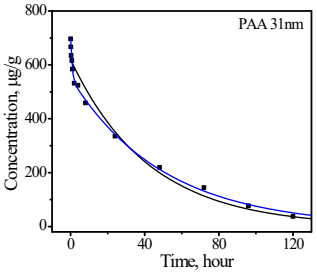
PAA 31nm
Concentration, µg/g
Time, hour

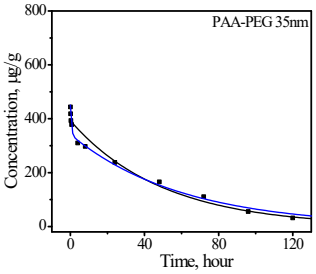
PAA-PEG 35nm
Concentration, µg/g
Time, hour

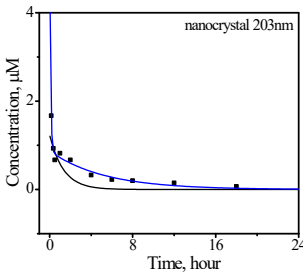

Fig. S1. The curve fitting of NPs data for parameterization based on one- (black curve) and two-compartment (blue curve) kinetics.

1 Methods

1.1 The derivation of total rate constants

Fig. 1 shows different pathways for clearance of NPs from blood. For example, in liver capillaries, NPs in bloodstream could penetrate into organs and be taken up by macrophages. The priorities and contributions of pathways are unclear. We assume NPs fluid as electric current, and different pathways for clearance as parallel resistors (Fig. S2).

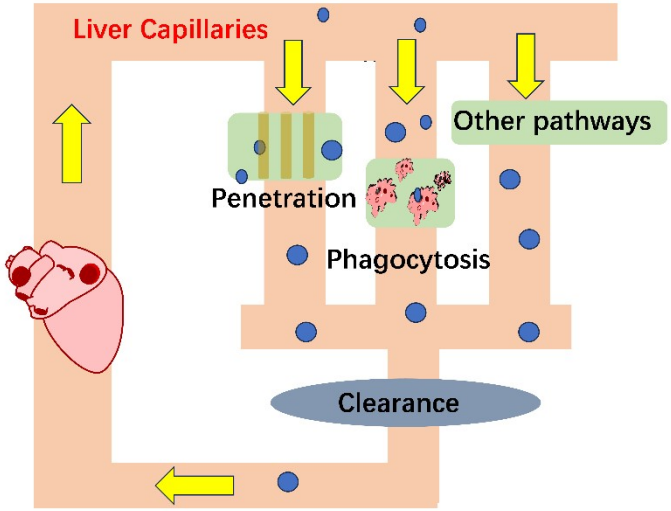

Fig. S2 Different clearance pathways in liver capillaries in parallel.

According to Ohm's law, the total effects of various pathways (resistance) could be quantified as:

$$\frac{1}{k} = \frac{1}{k_{penetration}} + \frac{1}{k_{phagocytosis}} + \frac{1}{k_{others}} \cdots \quad \text{S1}$$

Since we only consider penetration and phagocytosis pathways, the Eq. S1 could be transformed as Eq. S2:

$$k = \frac{k_{penetration} \cdot k_{phagocytosis}}{k_{penetration} + k_{phagocytosis}} \quad \text{S2}$$

1.2 Clearance rate constants based on *Van der Waals* energy

The two-compartment kinetic assumes that NPs undergo different distribution in central compartment and peripheral compartment. We assume the clearance of NPs in central compartment would be associated with the uptake of the reticuloendothelial system. However, the clearance of NPs in peripheral compartment may involve more complex mechanisms. Hence, we generically stipulate that clearance rate constants (k_c) based on two-compartment kinetics could be described via activation energy E_a

between NPs and phagocytes (e.g., macrophages) as Arrhenius equation and collision theory

$$k_c = Z_m \cdot \rho \cdot \exp^{(-Ea/k_B T)} \quad \text{(S3)}$$

in which Z_m is collision frequency, unit collisions/s in 1 m^3 of solution, ρ is the steric factor and $e^{-Ea/(k_B \cdot T)}$ [b]is the effective fraction of collision with energy than the activation energy. k_BT is the product of Boltzmann's constant k_B and temperature T (310K). However, blood clearance of NPs is based on complex mechanisms, and we were unable to calculate the exact activation energy. We proposed a potential energy (ΔG) which would influence the clearance process. ΔG are the potential part of *Ea*, and could be described as

$$Ea = \delta_1 \cdot \Delta G_1 + \delta_2 \cdot \Delta G_2 + \delta_3 \cdot \Delta G_3 + \cdots \quad \text{(S4)}$$

where δ is the influence coefficient of different potential energies (ΔG) on the total activation energy *Ea*. We obtained one of ΔG by calculating interaction energy involving *Van de Waals* interaction energy ($\Delta G_{LW}(h)$) according to [1]

$$\Delta G_{LW}(h) = \frac{\pi h_0^{\,2} \Delta G^{LW} r_{np}}{h(1+11.12h/\lambda_c)} \quad \text{(S5)}$$

where ΔG^{LW} is the Lifshitz-van de Waals free energy of interaction between NPs and macrophages in water, $\Delta G^{LW} = (\sqrt{\gamma_{np}^{\,LW}} - \sqrt{\gamma_m^{\,LW}})^2 - (\sqrt{\gamma_{np}^{\,LW}} - \sqrt{\gamma_{water}^{\,LW}})^2 - (\sqrt{\gamma_m^{\,LW}} - \sqrt{\gamma_{water}^{\,LW}})^2$, where $\gamma_{np}^{\,LW}$, $\gamma_m^{\,LW}$ and $\gamma_{water}^{\,LW}$ are Van de Waals free energies of NPs, macrophages and water) at distance *h_0*, which is the minimum equilibrium distance due to Born repulsion, 0.157 nm. r_{np} is the particle radius. *h* is the separation distance between the interacting surfaces (here we calculate $\Delta G^{LW}(h)$ when $h=h\_0$) and λ_c is the characteristic wavelength of the interaction, which is often assumed to be 100 nm.

The surface free energy components of NPs (the Lifshitz-van de Waals ($\gamma_{np}^{\,LW}$) [1] based on coating compounds were obtained by calculating single molecular weight per molecular volume and topological polar surface area per volume. Values for surface free energy components of PEG were obtained from measurements by Van Oss et al. [2]. All coating compounds' identifiers (i.e., SMILE strings) are shown in Table S1. The γ^{LW}_{cell} are defined as 30 mJ/m^2 for macrophages surface [3].

We combined Eqs. S3-5 and transform it to logarithmic form as

$$\ln(k_c) = \ln(Z_m) + \ln(\rho) + \delta \cdot \Delta G_{LW}(h) \quad \text{S6}$$

Table S1. The fitting results of data points for parameterization and validation based on one- and two-compartment kinetics.

NP	One-compartment kinetic			Two-compartment kinetic		
	$C(t)=C(0)\cdot e^{kt}+C(\infty)$, k ($h^{-1}$), C ($\mu(n)g\cdot g^{-1}(mL^{-1})$)	R^2	*P* value	$C(t)=C_c(0)\cdot e^{k_c t}+C_p(0\cdot e^{-k_p t}$, k_c and k_p (h^{-1}), C ($\mu(n)g\cdot g^{-1}(mL^{-1})$)	R^2	*P* value
QDPEG5000/2000 [4]	$C(t)=220.0\cdot e^{(-3.18t)}$	0.98	<0.001	$C(t)=3280.7\cdot e^{(-1.78t)}-3068.6\cdot e^{(-1.71t)}$	0.99	<0.001
QD-CdTe/CdS [5]	$C(t)=20.6\cdot e^{(-0.08t)}+2.6$	1.00	<0.001	$C(t)=20.6\cdot e^{(-0.08t)}+2.6\cdot e^{(0.00t)}$	1.00	<0.001
Au/ Poly(amidoamine) dendrimer composite nanodevices [6]	$C(t)=160.8\cdot e^{(-0.83t)}$	0.97	0.014	$C(t)=120.8\cdot e^{(-1.45t)}+43.1\cdot e^{(-0.03t)}$	1.00	NAN
Au/ Poly(amidoamine) dendrimer composite nanodevices [6]	$C(t)=127.3\cdot e^{(-2.90t)}$	0.98	0.010	$C(t)=203.1\cdot e^{(-10.00t)}+9.0\cdot e^{(-0.01t)}$	1.00	NAN
$Cu_{2-x}Se$ NP [7]	$C(t)=48.3\cdot e^{(-0.49t)}+5.8$	0.97	<0.001	$C(t)=42.6\cdot e^{(-0.85t)}+16.2\cdot e^{(-0.06t)}$	1.00	<0.001
QD-CdTe [8]	$C(t)=4.2\cdot e^{(-0.03t)}$	1.00	0.002	$C(t)=2.2\cdot e^{(-0.06t)}+2.1\cdot e^{(-0.02t)}$	1.00	NAN
AuNP [9]	$C(t)=1.6\cdot e^{(-0.09t)}$	0.78	<0.001	$C(t)=1.8\cdot e^{(-5.80t)}+1.1\cdot e^{(-0.04t)}$	0.93	0.001
ZnO [10]	$C(t)=4.1\cdot e^{(-0.69t)}+0.7$	0.93	<0.001	$C(t)=4.3\cdot e^{(-0.80t)}+0.8\cdot e^{(-0.00t)}$	0.98	<0.001
ZnO [10]	$C(t)=2.9\cdot e^{(-0.34t)}+0.4$	0.91	0.001	$C(t)=2.9\cdot e^{(-0.50t)}+0.8\cdot e^{(-0.01t)}$	0.98	<0.001
IONPs-PEG2000 [11]	$C(t)=236.4\cdot e^{(-2.34t)}$	0.97	<0.001	$C(t)=1118.3\cdot e^{(-2.34t)}-881.8\cdot e^{(-2.34t)}$	0.97	0.002
IONPs-PEG5000 [11]	$C(t)=177.0\cdot e^{(-2.23t)}+35.0$	0.98	0.002	$C(t)=164.5\cdot e^{(-3.41t)}+62.3\cdot e^{(-0.12t)}$	0.99	0.004
IONPs- PEG5000 [11]	$C(t)=213.3\cdot e^{(-1.72t)}$	0.95	<0.001	$C(t)=173.9\cdot e^{(-6.30t)}+99.0\cdot e^{(-0.60t)}$	0.99	0.009
Poly(lactide-co-glycolide)-mPEG256-5000 [12]	$C(t)=50.2\cdot e^{(-0.30t)}+22.7$	0.99	0.008	$C(t)=72.6\cdot e^{(-0.18t)}-0.0\cdot e^{(1.52t)}$	1.00	0.027
Poly(lactide-co-glycolide)-mPEG153-5000 [12]	$C(t)=20.2\cdot e^{(-0.90t)}+58.3$	0.86	0.142	$C(t)=69.3\cdot e^{(-4.00t)}+10.2\cdot e^{(-0.04t)}$	0.96	0.037
Poly(lactide-co-glycolide)-mPEG61-5000 [12]	$C(t)=36.4\cdot e^{(-0.45t)}+39.0$	0.99	0.006	$C(t)=72.9\cdot e^{(-0.19t)}+2.0\cdot e^{(0.39t)}$	1.00	0.011
Poly(lactide-co-glycolide)-mPEG34-5000 [12]	$C(t)=40.5\cdot e^{(-0.72t)}+23.1$	0.98	0.023	$C(t)=45.3\cdot e^{(-2.20t)}+19.7\cdot e^{(-0.10t)}$	1.00	0.010
PAA(Polyacrylamide) [13]	$C(t)=619.5\cdot e^{(-0.02t)}$	0.97	<0.001	$C(t)=550.8\cdot e^{(-1.30t)}+154.2\cdot e^{(-0.02t)}$	1.00	<0.001
PAA-PEG [13]	$C(t)=392.2\cdot e^{(-0.02t)}$	0.96	<0.001	$C(t)=341.3\cdot e^{(-1.86t)}+113.0\cdot e^{(-0.02t)}$	1.00	<0.001
Nanocrystal-SNX-2112 [14]	$C(t)=1.2\cdot e^{(-0.75t)}+0.2$	0.82	0.002	$C(t)=4.9\cdot e^{(-12.00t)}+0.9\cdot e^{(-0.20t)}$	0.98	<0.001

AuNP-PEG5000 [15]	$C(t)=2502.0\cdot e^{(-0.13t)}$	0.99	<0.001	$C(t)=2094.1\cdot e^{(-0.21t)}+511.1\cdot e^{(-0.02t)}$	1.00	<0.001
AuNP-PEG5000 [15]	$C(t)=6517.0\cdot e^{(-0.02t)}$	0.98	<0.001	$C(t)=6299.2\cdot e^{(-4.27t)}+6162.7\cdot e^{(-0.01t)}$	0.99	0.001
QD705-PEG5000 [16]	$C(t)=22.1\cdot e^{(-0.05t)}$	1.00	<0.001	$C(t)=19.0\cdot e^{(-0.05t)}+3.0\cdot e^{(-0.02t)}$	1.00	<0.001
QD705-PEG5000 [16]	$C(t)=11.1\cdot e^{(-0.05t)}$	1.00	<0.001	$C(t)=10.1\cdot e^{(-0.05t)}+1.0\cdot e^{(-0.01t)}$	1.00	<0.001
AuNP-PEG [17]	$C(t)=11.1\cdot e^{(-0.29t)}-0.21$	0.97	0.17	--	--	--
AuNP-PEG [18]	*k=0.10	--	--	--	--	--
AuNP-Trimethylammonium groups and sulfonic groups [18]	*k=0.02	--	--	--	--	--
AuNP -Citric acid-PEG-Thioctic acid [19]	*k=1.41	--	--	--	--	--
AuNP -Citric acid-PEG-Thioctic acid [19]	*k=0.53	--	--	--	--	--
AuNP -Citric acid-PEG-Thioctic acid [19]	*k=0.87	--	--	--	--	--
AuNP-Dextran [20]	$C(t)=1.3\cdot e^{(-9.63t)}+0.0$	1	<0.001	--	--	--
Graphene oxide--PEG-NH2,p-SCN-Bn-NOTA (i.e., 2-S-(4-isothiocyanatobenzyl)-1,4,7-triazacyclononane-1,4,7-triacetic acid) and FSHR-mAb-SH [21]	$C(t)=4.1\cdot e^{(-0.05t)}$	0.98	0.002	--	--	--
64Cu-Multifunctional mesoporous silica NP-800CW (fluorescence [NIRF] dye)-human/murine chimeric IgG1 monoclonal antibody (TRC105) [22]	$C(t)=4.0\cdot e^{(-0.02t)}$	0.78	0.003	--	--	--
64Cu-NOTA-Hollow mesoporous silica NP-ZW800-PEG-TRC105 [23]	$C(t)=1.3\cdot e^{(-0.22t)}+3.8$	1	0.024	--	--	--
Cy5 dye-encapsulating core-shell silica NP [24]	$C(t)=18.7\cdot e^{(-0.12t)}+0.2$	1	<0.001	--	--	--
IONPs-N-(trimethoxysilylpropyl)ethylenediaminetriacetate trisodium salt [25]	$C(t)=78.8\cdot e^{(-8.22t)}+1.6$	1	<0.001	--	--	--
DL-Poly(L-lactide) NP [26]	--	--	--	$C(t)=31.5\cdot e(-2.77t)+31.2\cdot e(-0.09t)$	0.98	<0.001
PEG- Poly(L-lactide)-PEG NP [26]	--	--	--	$C(t)=2.9\cdot e(-1.08t)+14.5\cdot e(-0.01t)$	0.98	<0.001
Methoxy-PEG-poly(lactide-*co*-glycolide)-PEG-Methoxy (PELGE) [27]	--	--	--	$C(t)=3.8\cdot e(-2.31t)+3.2\cdot e(-0.02t)$	0.95	<0.001
Yb_2O_3-Silanated m-PEG [28]	--	--	--	$C(t)=11.8\cdot e(-1.65t)+8.2\cdot e(-0.08t)$	0.99	<0.001

* denotes data values were obtained from original studies.

Table S2. Chemical information of NPs coatings (including 7 data points for parameterization and 4 data points for validation (in bold)).

NP	SMILE	TPSA	MW	Volume	γ^{LW}, J/m^2	γ^{+}, J/m^2	γ^{-}, J/m^2
IONPs-PEG5000	OCCO	NAN	NAN	NAN	43.00	0.43	64.00[2]
IONPs-PEG5000	OCCO	NAN	NAN	NAN	43.00	0.43	64.00
PLGA-mPEG153-5000	COCCOC(=O)COC(=O)C(C)O	82.07	206.19	185.93	35.47	1.11	29.94
PLGA-mPEG34-5000	COCCOC(=O)COC(=O)C(C)O	82.07	206.19	185.93	35.47	1.11	29.94
PAA-PEG	C=CC(=O)NOCCO	58.56	131.13	122.36	33.94	1.22	32.98
PAA	C=CC(=O)N	43.09	71.08	70.64	31.26	1.61	43.74
Nanocrystal- SNX-2112	CC1(CC2=C(C(=O)C1)C(=NN2C3=CC(=C(C=C3)C(=O)N)NC4CCC(CC4)O)C(F)(F)F)C	110.25	464.49	400.04	37.60	0.61	16.35
D=La(PLA)	C(=O)C(C)O	537.09	1443.28	1238.81	37.76	1.08	29.31
PEG-PLA-PEG	COCCOCCOCCOCCOCCOC(=O)C(C)OC(=O)C(C)OC(=O)C(C)OC(=O)C(C)OC(=O)C(C)OC(=O)C(C)OC(=O)C(C)OC(=O)NCCCCCCNC(=O)OC(C)C(=O)OC(C)C(=O)OC(C)C(=O)OC(C)C(=O)OC(C)C(=O)OC(C)C(=O)OC(C)C(=O)OC(C)C(=O)OC(C)C(=O)OC(C)C(=O)OCCOCCOCCOC COCCOC	563.58	1753.76	1573.55	35.70	0.86	23.11
PELGE	COCCOCOCOCOC(C)OC(=O)NCCCCCCNC(=O)OC(C)OCOCOCOCCOC	169	588.65	551.95	33.73	0.70	18.84
Silanated m-PEG	COCCOCCOC(O)NCCCCCCNC(O)OCCCCCCCCC CCSCCC[Si]OC	110.68	596.95	620.10	29.48	0.32	8.34

Reference

1. B. Q. Lu, A. J. Hendriks and T. M. Nolte, A generic model based on the properties of nanoparticles and cells for predicting cellular uptake, *Colloids and Surfaces B-Biointerfaces*, 2022, **209**.
2. C. J. Vanoss, M. K. Chaudhury and R. J. Good, MONOPOLAR SURFACES, *Adv. Colloid Interface Sci.*, 1987, **28**, 35-64.
3. T. M. Nolte, B. Q. Lu and A. J. Hendriks, Nanoparticles in bodily tissues: predicting their equilibrium distributions, *Environmental Science-Nano*, 2022, DOI: 10.1039/d2en00469k.
4. E. Yaghini, E. Tacconi, A. Pilling, P. Rahman, J. Broughton, I. Naasani, M. R. S. Keshtgar, A. J. MacRobert and O. Della Pasqua, Population pharmacokinetic modelling of indium-based quantum dot nanoparticles: preclinical in vivo studies, *Eur. J. Pharm. Sci.*, 2021, **157**.
5. X. W. Liang, H. L. Wang, J. E. Grice, L. Li, X. Liu, Z. P. Xu and M. S. Roberts, Physiologically Based Pharmacokinetic Model for Long-Circulating Inorganic Nanoparticles, *Nano Lett.*, 2016, **16**, 939-945.
6. D. E. Mager, V. Mody, C. Xu, A. Forrest, W. G. Lesniak, S. S. Nigavekar, M. T. Kariapper, L. Minc, M. K. Khan and L. P. Balogh, Physiologically Based Pharmacokinetic Model for Composite Nanodevices: Effect of Charge and Size on In Vivo Disposition, *Pharm. Res.*, 2012, **29**, 2534-2542.
7. Y. B. Han, T. T. Wang, H. H. Liu, S. H. Zhang, H. Zhang, M. T. Li, Q. Sun and Z. Li, The release and detection of copper ions from ultrasmall theranostic Cu2-xSe nanoparticles, *Nanoscale*, 2019, **11**, 11819-11829.
8. K. C. Nguyen, Y. Zhang, J. Todd, K. Kittle, D. Patry, D. Caldwell, M. Lalande, S. Smith, D. Parks, M. Navarro, A. Massarsky, T. W. Moon, W. G. Willmore and A. F. Tayabali, Biodistribution and Systemic Effects in Mice Following Intravenous Administration of Cadmium Telluride Quantum Dot Nanoparticles, *Chem. Res. Toxicol.*, 2019, **32**, 1491-1503.
9. F. Naz, V. Koul, A. Srivastava, Y. K. Gupta and A. K. Dinda, Biokinetics of ultrafine gold nanoparticles (AuNPs) relating to redistribution and urinary excretion: a long-term in vivo study, *J. Drug Targeting*, 2016, **24**, 720-729.
10. W. Y. Chen, Y. H. Cheng, N. H. Hsieh, B. C. Wu, W. C. Chou, C. C. Ho, J. K. Chen, C. M. Liao and P. Lin, Physiologically based pharmacokinetic modeling of zinc oxide nanoparticles and zinc nitrate in mice, *Int. J. Nanomed.*, 2015, **10**, 6277-6292.
11. W. M. Xue, Y. Y. Liu, N. Zhang, Y. D. Yao, P. Ma, H. Y. Wen, S. P. Huang, Y. N. Luo and H. M. Fan, Effects of core size and PEG coating layer of iron oxide nanoparticles on the distribution and metabolism in mice, *Int. J. Nanomed.*, 2018, **13**, 5719-5731.
12. K. Avgoustakis, A. Beletsi, Z. Panagi, P. Klepetsanis, E. Livaniou, G. Evangelatos and D. S. Ithakissios, Effect of copolymer composition on the physicochemical characteristics, in vitro stability, and biodistribution of PLGA-mPEG nanoparticles, *Int. J. Pharm.*, 2003, **259**, 115-127.
13. Y. Wenger, R. J. Schneider, G. R. Reddy, R. Kopelman, O. Jolliet and M. A. Philbert, Tissue distribution and pharmacokinetics of stable polyacrylamide nanoparticles following intravenous injection in the rat, *Toxicol. Appl. Pharmacol.*, 2011, **251**, 181-190.
14. D. Dong, X. Wang, H. L. Wang, X. W. Zhang, Y. F. Wang and B. J. Wu, Elucidating the in vivo fate of nanocrystals using a physiologically based pharmacokinetic model: a case study with the anticancer agent SNX-2112, *Int. J. Nanomed.*, 2015, **10**, 2521-2535.

15. W. S. Cho, M. Cho, J. Jeong, M. Choi, B. S. Han, H. S. Shin, J. Hong, B. H. Chung, J. Jeong and M. H. Cho, Size-dependent tissue kinetics of PEG-coated gold nanoparticles, *Toxicol. Appl. Pharmacol.*, 2010, **245**, 116-123.
16. R. H. Yang, L. W. Chang, J. P. Wu, M. H. Tsai, H. J. Wang, Y. C. Kuo, T. K. Yeh, C. S. Yang and P. Lin, Persistent tissue kinetics and redistribution of nanoparticles, quantum dot 705, in mice: ICP-MS quantitative assessment, *Environ. Health Perspect.*, 2007, **115**, 1339-1343.
17. Arnida, M. M. Janát-Amsbury, A. Ray, C. M. Peterson and H. Ghandehari, Geometry and surface characteristics of gold nanoparticles influence their biodistribution and uptake by macrophages, *European Journal of Pharmaceutics and Biopharmaceutics*, 2011, **77**, 417-423.
18. X. S. Liu, H. Li, Y. J. Chen, Q. Jin, K. F. Ren and J. Ji, Mixed-Charge Nanoparticles for Long Circulation, Low Reticuloendothelial System Clearance, and High Tumor Accumulation, *Advanced Healthcare Materials*, 2014, **3**, 1439-1447.
19. G. D. Zhang, Z. Yang, W. Lu, R. Zhang, Q. Huang, M. Tian, L. Li, D. Liang and C. Li, Influence of anchoring ligands and particle size on the colloidal stability and in vivo biodistribution of polyethylene glycol-coated gold nanoparticles in tumor-xenografted mice, *Biomaterials*, 2009, **30**, 1928-1936.
20. A. L. Bailly, F. Correard, A. Popov, G. Tselikov, F. Chaspoul, R. Appay, A. Al-Kattan, A. V. Kabashin, D. Braguer and M. A. Esteve, In vivo evaluation of safety, biodistribution and pharmacokinetics of laser-synthesized gold nanoparticles, *Scientific Reports*, 2019, **9**.
21. D. Z. Yang, L. Z. Feng, C. A. Dougherty, K. E. Luker, D. Q. Chen, M. A. Cauble, M. M. B. Holl, G. D. Luker, B. D. Ross, Z. Liu and H. Hong, In vivo targeting of metastatic breast cancer via tumor vasculature-specific nano-graphene oxide, *Biomaterials*, 2016, **104**, 361-371.
22. F. Chen, T. R. Nayak, S. Goel, H. F. Valdovinos, H. Hong, C. P. Theuer, T. E. Barnhart and W. B. Cai, In Vivo Tumor Vasculature Targeted PET/NIRF Imaging with TRC105(Fab)-Conjugated, Dual-Labeled Mesoporous Silica Nanoparticles, *Mol. Pharm.*, 2014, **11**, 4007-4014.
23. F. Chen, H. Hong, S. X. Shi, S. Goel, H. F. Valdovinos, R. Hernandez, C. P. Theuer, T. E. Barnhart and W. B. Cai, Engineering of Hollow Mesoporous Silica Nanoparticles for Remarkably Enhanced Tumor Active Targeting Efficacy, *Scientific Reports*, 2014, **4**.
24. M. Benezra, O. Penate-Medina, P. B. Zanzonico, D. Schaer, H. Ow, A. Burns, E. DeStanchina, V. Longo, E. Herz, S. Iyer, J. Wolchok, S. M. Larson, U. Wiesner and M. S. Bradbury, Multimodal silica nanoparticles are effective cancer-targeted probes in a model of human melanoma, *J. Clin. Invest.*, 2011, **121**, 2768-2780.
25. Z. Z. Sun, M. Worden, J. A. Thliveris, S. Hombach-Klonisch, T. Klonisch, J. van Lierop, T. Hegmann and D. W. Miller, Biodistribution of negatively charged iron oxide nanoparticles (IONPs) in mice and enhanced brain delivery using lysophosphatidic acid (LPA), *Nanomedicine-Nanotechnology Biology and Medicine*, 2016, **12**, 1775-1784.
26. X. Q. Shan, C. S. Liu, Y. Yuan, F. Xu, X. Y. Tao, Y. Sheng and H. J. Zhou, In vitro macrophage uptake and in vivo biodistribution of long-circulation nanoparticles with poly(ethylene-glycol)-modified PLA (BAB type) triblock copolymer, *Colloids and Surfaces B-Biointerfaces*, 2009, **72**, 303-311.
27. Y. R. Duan, J. P. Xu, Y. Z. Lin, H. Yu, T. Gong, Y. G. Li and Z. R. Zhang, A preliminary study on MeO-PEG-PLGA-PEG-OMe nanoparticles as intravenous carriers, *Journal of Biomedical Materials Research Part A*, 2008, **87A**, 515-523.

28. Z. Liu, Z. H. Li, J. H. Liu, S. Gu, Q. H. Yuan, J. S. Ren and X. G. Qu, Long-circulating Er3+-doped Yb2O3 up-conversion nanoparticle as an in vivo X-Ray CT imaging contrast agent, *Biomaterials*, 2012, **33**, 6748-6757.